Scientific Reports

https://doi.org/10.1038/s41598-026-45487-0

Article in Press

High gain and slant dual-polarized antenna for private 5G railway base stations

Received: 18 January 2026

Accepted: 19 March 2026

Published online: 26 March 2026

Cite this article as: Lee J., Han Y. & Ahn B.K. High gain and slant dual-polarized antenna for private 5G railway base stations. *Sci Rep* (2026). https://doi.org/10.1038/s41598-026-45487-0

Jae-Geun Lee, Youjin Han & Byung Kuon Ahn

High Gain and Slant Dual-Polarized Antenna for Private 5G Railway Base Stations

Jae-Geun Lee[1], **Youjin Han**[1], **and Byung Kuon Ahn**[1,2,*]

[1]Department of Intelligent Semiconductors, Soongsil University, Seoul, 06978, South Korea
[2]School of Electronic Engineering, Soongsil University, Seoul, 06978, South Korea
[*]abg6312@ssu.ac.kr

ABSTRACT

This paper proposes a novel antenna structure that simultaneously satisfies high gain, dual-polarization, and fan-beam radiation pattern characteristics for Private 5G base stations in next-generation railway communications. In Private 5G railway communications, a balance of high gain, dual-polarization, and fan-beam is crucial. High gain and fan-beam pattern maximize coverage along the track, while dual-polarization provides link robustness for high-speed mobility. The proposed antenna element achieves a high gain of 12.8 dBi and stable radiation performance despite its relatively compact size by employing a radiation mechanism based on a higher-order mode patch antenna and a sidelobe suppression technique utilizing central and side slots. Furthermore, by rotating the antenna by 45° and configuring it in a slant dual-polarization structure, it provides robustness against polarization variations that frequently occur in practical communication environments. A 6×1 array antenna constructed based on the proposed antenna element forms a stable fan-beam radiation pattern with suppressed grating lobes even at wide array spacing of $1.27\lambda_0$, providing a horizontal half-power beamwidth (HPBW) of 6°, a vertical HPBW of 38°, and a peak gain of 18.6 dBi. The 6-way power divider designed for dual-polarization array feeding ensures excellent uniform power distribution with an insertion loss deviation within ±0.32 dB and an insertion phase deviation within ±2.8°. Both the proposed antenna element and the array antenna achieve sufficient bandwidth coverage for the Private 5G band, demonstrating performance suitable for application in practical base station environments. Moreover, a figure-of-merit comparison defined based on peak gain, fractional bandwidth, and antenna size confirms that the proposed antenna achieves the most balanced performance compared to previously reported high gain dual-polarized antennas. These results indicate that the proposed antenna can provide high reliability for next-generation Private 5G railway base stations and offer significant advantages in terms of coverage, interference mitigation, and link robustness in practical railway operating environments.

Introduction

Recently, discussions on next-generation railway communication technology based on the 5G band are actively underway in many countries[1]. In South Korea, Private 5G-R (Railway) has been designated as a next-generation railway communication band, providing a bandwidth of 100 MHz in the 4.7 GHz band. This is a significantly expanded spectrum resource compared to the LTE-R (Long-Term Evolution-Railway) system, which uses only 20 MHz bandwidth in the 700 MHz band[2]. The expanded bandwidth enables low latency, high data rates, and enhanced reliability, enabling various smart railway services such as in-vehicle ultra-high-definition streaming, real-time security video transmission, real-time information exchange between infrastructure and trains, and remote maintenance[3]. This paper aims to design a base station antenna that reflects practical operation scenarios to support next-generation railway communications. The high frequency band of Private 5G inevitably increases the attenuation of signals in the air, so high gain characteristic is essential to compensate for this. At the same time, the various topographical and spatial characteristics around trains create various scenarios, such as viaducts, hills, tunnels, urban areas, railway stations, mountainous terrain, and inter-train communications. Most of these communication environments can be treated as Line-of-Sight (LoS) scenarios, but some environments such as urban areas, railway stations, mountainous terrain, and inter-train communications can be partially considered Non-Line-of-Sight (NLoS) scenarios due to obstacles[4]. In NLoS, communication environments, various obstacles cause propagation mechanisms such as reflection, refraction, and diffraction, which change the original polarization state of the radio wave[5,6]. Accordingly, antennas should be designed to support dual-polarization in order to effectively receive the signals with altered polarization states.

The communication environments, antenna gain, and beam patterns have a significant impact on the performance of wireless communication systems, including coverage, link robustness, and throughput. Therefore, antenna characteristics should be selected based on the railway communication environment, considering the trade-off relationship between antenna gain and beamwidth. In general, antennas with high gain narrow pencil-beam radiation pattern exhibit good communication performance in LoS environments. However, in NLoS environments with dense obstacles, antennas with moderate gain and a wide fan-beam

radiation pattern exhibit better communication performance. These two types of antennas are specialized for their respective environments, limiting their general usability. Therefore, an antenna with high gain, dual-polarization, and fan-beam pattern demonstrate balanced performance in both LoS and NLoS environments. Antennas for next-generation railway communications should be designed to reflect these characteristics. The primary objective of the antenna design proposed in this paper is to implement a high gain fan-beam pattern antenna that can minimize interference-sensitive zones and provide concentrated signals to Private 5G service areas while satisfying government railway communication regulations. The areas near railways must suppress unnecessary radiation and ensure sufficient coverage along the tracks, as base station output and beam pattern can interfere with nearby commercial 5G systems. This perspective is also supported by previous 5G antenna performance analysis studies[7,8], which report that high gain pencil-beam antennas are advantageous in achieving high reference signal received power (RSRP) and extended coverage in long-range LoS scenarios. However, these studies also indicate that excessively narrow beamwidth can result in severe throughput degradation under NLoS conditions or when receiver positioning deviations occur. Previous studies have focused on LoS-centric optimization in railway environments, often employing pencil-beam patterns with horizontal and vertical HPBW of 6°[8–13]. However, in railway communication environments where NLoS is frequent, these highly directive beam patterns result in significant spatial variation in signal strength, degrading link robustness and throughput. In order to address these issues, this paper proposes a high gain dual-polarized antenna with a fan-beam pattern with a horizontal HPBW of 6° and vertical HPBW of 40° to provide balanced performance in practical railway communication environments.

Despite many research on antennas for next-generation railway communications have been proposed, achieving a well-balanced performance of high gain, dual-polarization, and fan-beam radiation pattern remains challenging[14–23]. Magneto-electric dipole antennas[14,15] and dielectric resonator antennas[16,17] satisfy high gain and dual-polarization, but their bulky size makes them difficult for practical applications. Microstrip patch antennas have been extensively studied to achieve high gain and dual-polarization due to their advantages of low profile, low cost, and ease of integration with planar circuits[18–21]. Reference[18] employed a stacked structure to achieve high isolation, a subarray structure to increase gain, and a symmetrical structure for dual-polarization. However, the stacked structure increases the effective permittivity, which reduces the effective aperture and consequently degrades the antenna gain. In references[19–21], a high-order mode and slot structure were applied to increase gain, and a symmetric structure was applied to implement dual-polarization. Their design processes share a common approach: a linearly polarized rectangular patch antenna is designed first, and then two patches are arranged orthogonally in a cross shape to achieve dual-polarization. Although such cross-shaped antennas can effectively realize dual-polarization, the resulting gain improvement is less significant than expected despite the enlarged effective aperture. In reference[19], although the physical area of a cross-shaped dual-polarized antenna increased by 2.34 times compared to a rectangular single-polarized antenna, the achieved gain remained at a similar level. Moreover, references[20,21] reported that the antenna gain was even reduced. These previous studies show that converting a rectangular patch into a cross-shaped structure can achieve dual-polarization, but the antenna gain does not improve correspondingly despite the increase in aperture.

In order to effectively overcome these limitations, this paper proposes a novel antenna that simultaneously achieves high gain, dual-polarization, and fan-beam radiation pattern. The proposed antenna element is designed to have high gain characteristic by using higher-order mode and slot structures to compensate for signal attenuation in the high-frequency band. Furthermore, considering the frequent polarization changes in urban and railway station environments, the proposed antenna element is designed to have a 45° slant dual-polarization characteristic, which is the most advantageous structure for a base station antenna[22–24]. A linear array antenna is then designed by arranging six proposed antenna elements in a linear configuration. This array antenna is designed to have high gain, dual-polarization, and fan-beam pattern, achieving balanced performance in both LoS and NLoS scenarios. The proposed array antenna can substantially improve the limitations of previously reported antennas while reflecting the practical railway communications. This paper is organized as follows. The first section introduces the research background, the motivation of this study, and the requirements for next-generation railway communication systems. The second section presents the detailed design process of the proposed antenna element and array antenna, including their operating principles and theoretical basis. The third section presents the fabrication and measurement results of the prototype antennas, along with a performance analysis including comparisons with previous works. The final section summarizes the main contributions of this work and suggests future application directions.

Antenna Design

Fig. 1 illustrates the geometry of the proposed high gain dual-polarized antenna element. As shown in the figure, the proposed antenna consists of a multilayer printed circuit board (PCB) structure comprising a microstrip patch, an upper substrate, a supporting frame, a ground plane, a lower substrate, and a feed line. The upper and lower substrates are designed using the low loss substrate, Taconic RF-30 ($\varepsilon_r = 3.0$, $tan\delta = 0.0014$), with thicknesses of 1.52 mm and 0.76 mm, respectively. The patch, ground plane, and feed line are designed using copper with a thickness of 35 μm. The proposed antenna is designed as a suspended structure with an air gap between the radiating element and the ground plane, resulting in an effective permittivity

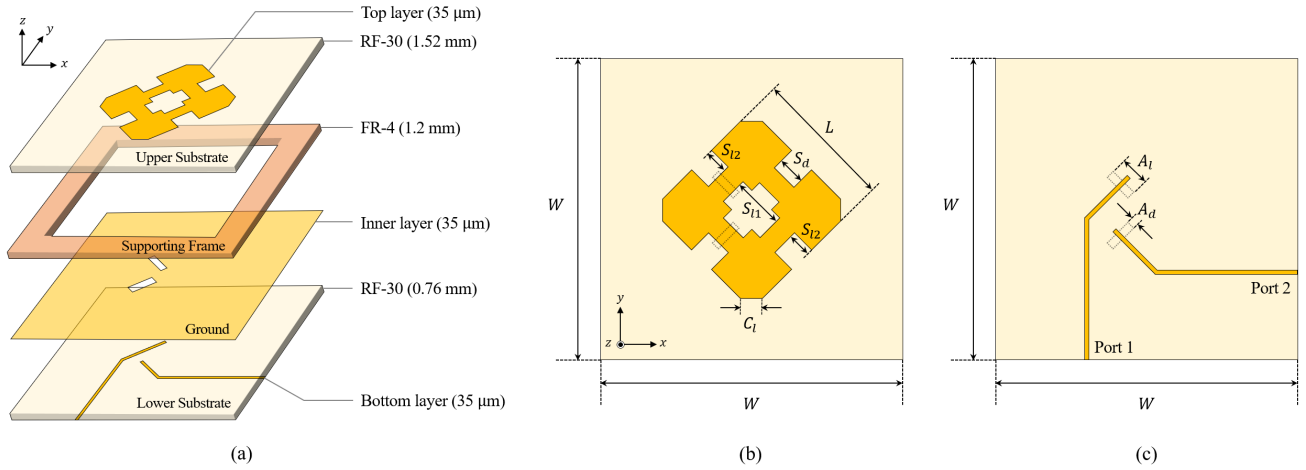

Figure 1. Geometry of the proposed antenna element. (a) Exploded view. (b) Top view of the top layer. (c) Top view of the bottom layer. Parameters: $W = 130$, $L = 61$, $S_{l1} = 22$, $S_{l2} = 11$, $S_d = 12$, $C_l = 10$, $A_d = 4$, $A_l = 13$, $N_{l1} = 4$, $N_{l2} = 14.5$ (unit: mm)

lower than that of the substrate. This structure allows for a larger effective aperture area at the same operating frequency, resulting in a higher gain antenna.

The supporting frame serves to form an air gap between the upper substrate and the ground plane. In the proposed structure, the supporting frame is designed using the substrate FR-4 ($\varepsilon_r = 4.3$, $tan\delta = 0.025$) with a thickness of 1.2 mm and a width of 20 mm, which supports only the edges of the antenna. The electrical characteristics of the supporting frame are not critical, so any material with a uniform thickness can be used. The microstrip patch on the top layer has a symmetrical structure with a cross-shaped slot in the center, four side slots along the edges, and truncated corners. The ground slot of the inner layer and the feed line of the bottom layer are designed to feed the antenna through aperture coupling. The positions of the ground slots in the xy-plane are equidistant from the center in the $\pm 45°$ directions. The design parameters were optimized using a three-dimensional electromagnetic (3D EM) simulator, and the detailed values are presented in the caption of Fig. 1.

Fig. 2 illustrates the design process of the proposed antenna, along with the corresponding electric field distribution and simulated gain for each antenna model. The ground slot and the feed line to feed each antenna model are indicated by dotted lines. The PCB stack-up, ground slot size, and feed line width of all antenna models are identical to those presented in Fig. 1, and the remaining parameters are presented in the caption of Fig. 2. All antenna models are designed as a suspended structure with an air gap between the ground plane and the upper substrate through a supporting frame. The Ant. 1 is a conventional square patch antenna operating in the fundamental TM_{01} mode, and its electric field distribution in the y-direction is shown in Fig. 2(b). As shown in the figure, Ant. 1, the conventional patch antenna, can be interpreted as a linear array of two radiating apertures spaced $0.5\lambda_0$ apart in the y-direction[25], where λ_0 is the free-space wavelength. The Ant. 2 is an antenna designed to operate in the higher-order resonant mode, TM_{03} mode, to increase antenna gain. The electric field distribution of Ant. 2 in the y-direction is shown in Fig. 2(c). As shown in the figure, Ant. 2 can be interpreted as a linear array of two radiating apertures spaced $1.5\lambda_0$ apart in the y-direction. Compared to Ant. 1, Ant. 2 exhibits a higher antenna gain due to the increased array spacing between the radiating apertures, but this also significantly increases the sidelobe level. Therefore, the gain enhancement relative to the increased antenna size is not as significant as expected. In order to address this issue, Ant. 3 adds a slot to the center of the TM_{03} mode patch antenna. As shown in Fig. 2(c), the center of the TM_{03} mode patch is the zero potential point where the voltage applied to the patch changes from positive to negative in the y-direction. By adding a slot at the center where zero potential exists, a new electric field distribution is formed from positive to negative voltage, whose orientation is aligned with the radiation direction of the originally formed apertures. Therefore, a linear array of four radiating apertures can be realized with a smaller array spacing than that of Ant. 2. Consequently, as shown in the electric field distribution of Ant. 3, it can be interpreted as a linear array of four radiating apertures spaced $0.5\lambda_0$ apart in the y-direction. Compared to Ant. 2, Ant. 3 shows an increase in antenna gain and a reduction in sidelobe level due to the increase in the number of radiating apertures and the decreased array spacing. Therefore, Ant. 3 effectively overcomes the shortcomings of higher-order mode patch antennas and achieves high gain. The Ant. 4 is a square structure with two Ant. 3 elements arranged along the x-direction. The electric field distribution in the y-direction of Ant. 4 is identical to that of Fig. 2(d), but it is arranged with a spacing of $0.5\lambda_0$ along the x-direction, which doubles the antenna gain. Fig. 2(e) shows the simulated gain of the four antenna models. Comparing Ant.1

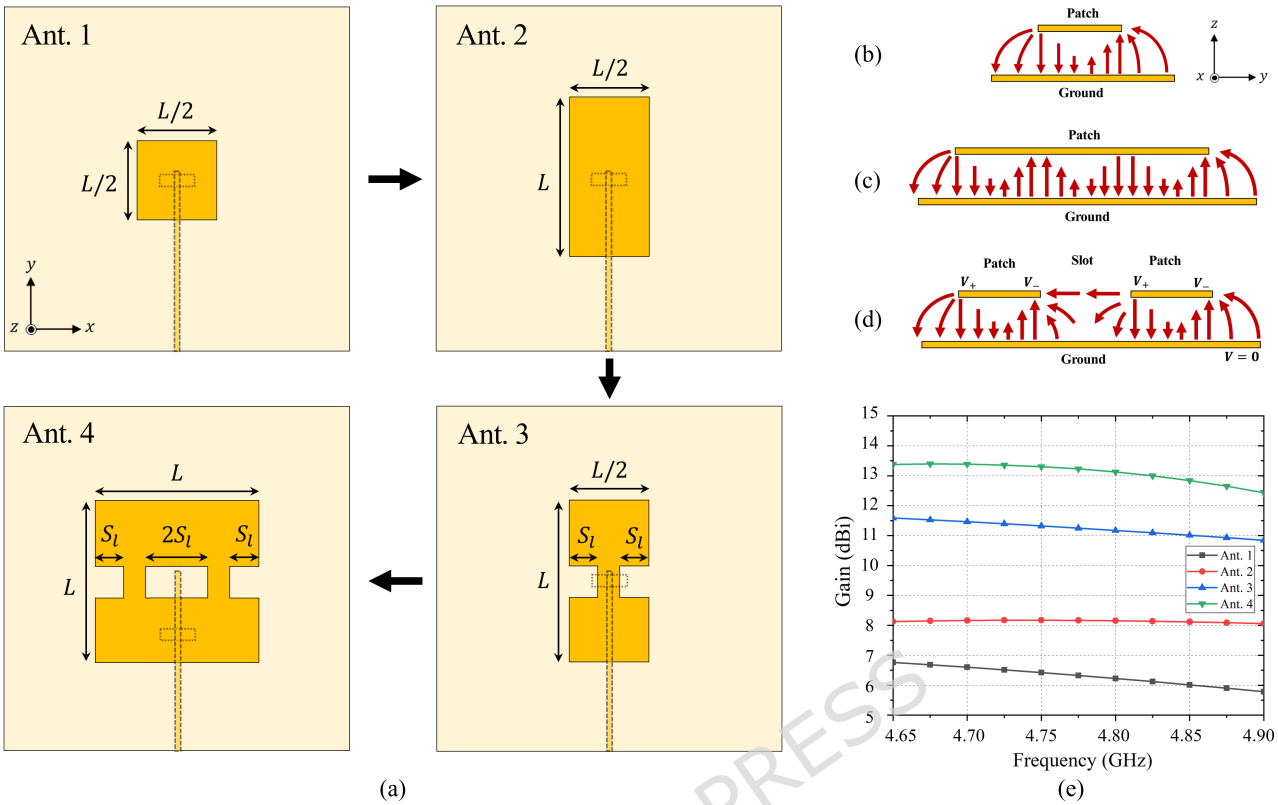

Figure 2. (a) Four antenna models in the design process of a high gain antenna. Illustrations of the electric field distribution of (b) Ant. 1, (c) Ant. 2, (d) Ant. 3 and Ant. 4. (e) Simulated gains of the four antenna models. Parameters: $L = 61$, $S_l = 11$ (unit: mm)

and Ant. 2, it can be seen that although higher-order mode operating increases the antenna gain, the gain enhancement is limited compared to the increase in antenna size. Comparing Ant. 2 and Ant. 3, it can be seen that adding slots to a patch antenna of the same size significantly increases antenna gain. Finally, comparing Ant. 3 and Ant. 4, it can be seen that the intended gain increase is also achieved by extending the antenna in the x-direction. These comparisons confirm the validity of the design process of each antenna stage. The Ant. 4 has a gain of 13 dBi, and a HPBW of 40° in both the xz-plane and yz-plane.

The design process for a dual-polarized antenna using the antenna model of Ant. 4 is illustrated in Fig. 3. The Ant. A has the same structure as Ant. 4 in Fig. 2, and Ant. B is an antenna model in which Ant. A is rotated 90° in the xy-plane. Since the feed directions are orthogonal to each other, Ant. A and Ant. B have vertical polarization (V-pol.) and horizontal polarization (H-pol.), respectively. The Ant. C, a combination of these two antenna models, operates as a high gain dual-polarization

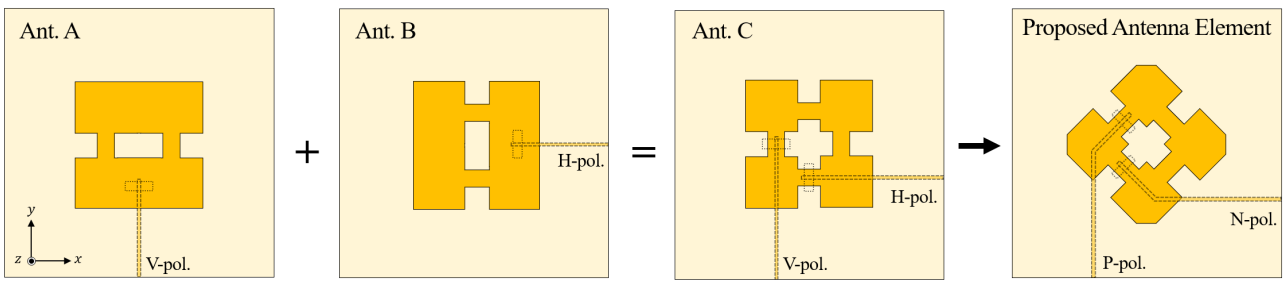

Figure 3. Design process of the slant dual-polarized antenna.

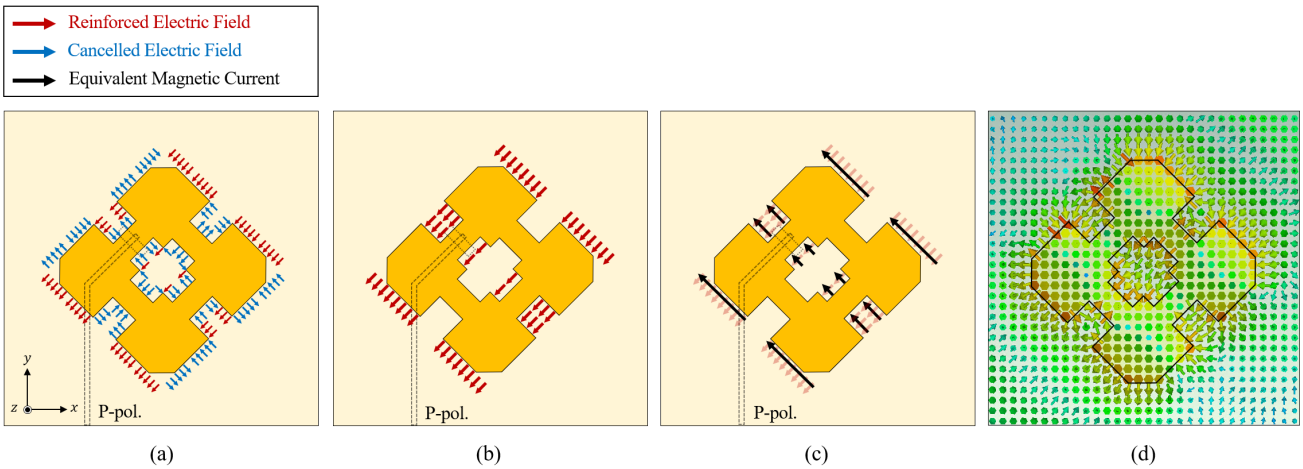

Figure 4. Electric field distributions of the proposed patch antenna element for P-pol. (a) Schematic illustration of the electric field distribution. (b) Schematic illustration of the reinforced electric field distribution. (c) Schematic illustration of the equivalent magnetic current distribution. (d) Simulated electric field distribution.

antenna supporting both V-pol. and H-pol. In order to avoid overlap with the ground slots, the positions of the two feed lines are slightly adjusted. In the structure of Ant. C, excitation of the V-pol. feed line produces the electric field distribution shown in Fig. 2(d) along the y-direction, resulting in high gain, while excitation of the H-pol. feed line produces an identical electric field distribution along the x-direction, also resulting in high gain. Therefore, dual-polarization and high gain characteristics can be achieved effectively. The final proposed design is a 45° rotated shape of the Ant. C, the most commonly used dual-polarization structure in base station antennas. It supports dual-polarization of the $+45°$ slant positive polarization (P-pol.) and the $-45°$ slant negative polarization (N-pol.). Additionally, because the fan-beam implementation required an additional array antenna design, the antenna corners are truncated to ensure flexibility in array spacing. The configuration and design parameters of the proposed antenna element are detailed in Fig. 1.

The electric field analysis of the proposed antenna element is presented in Fig. 4. Since the operating principles of the two polarizations are identical and orthogonal, only the P-pol. case is considered. Fig. 4(a) presents a simplified schematic illustration to aid in the analysis of the electric field distribution of the proposed antenna element. For clarity, the electric field distributions beneath the patch is omitted, and the electric field components that cause constructive and destructive interference are indicated by red and blue arrows, respectively. The electric field distributions at the truncated corners are decomposed into the red and blue arrows. The electric field components indicated by the red arrows reinforce each other through constructive interference due to their identical directions, whereas those indicated by the blue arrows cancel each other through destructive interference due to their opposite directions. Therefore, the electric field components indicated by the red arrows primarily contribute to the radiation of the proposed antenna element. Fig. 4(b) presents a simplified representation of the electric field components indicated by red arrows, which primarily contribute to antenna radiation. The electric field distribution in Fig. 2(d) discussed above represents a cross-sectional view of this reinforced electric field. Through this analysis, the proposed antenna element can be interpreted as a two-dimensional array consisting of twelve radiating apertures. The electric field radiating from these apertures can be modeled as equivalent magnetic currents using equation (1) based on the Huygens' Principle[25], where $\vec{M}$, $\hat{n}$, and $\vec{E}$ denote the equivalent magnetic current, the unit normal vector of the aperture, and the electric field, respectively.

$$\vec{M} = -\hat{n} \times \vec{E} \tag{1}$$

As shown in Fig. 4(c), the proposed antenna element can also be interpreted as a two-dimensional array of twelve equivalent magnetic currents. Furthermore, the high gain of the proposed antenna element is also explained from the perspective of the magnetic current array. Fig. 4(d) shows the simulated electric field distribution of the proposed antenna element. The distribution of the reinforced and canceled electric fields generated around the radiating element can be clearly observed. This validates the analysis based on the simplified schematic illustration of the electric field distribution in Fig. 4(a). The simulation results of the electric field distribution when N-pol. is fed are completely identical to those of Fig. 4(d) rotated 90°. The 90° difference in the electric field distributions generated by the two feeding methods clearly explains the orthogonal dual-polarization characteristic of the proposed antenna element.

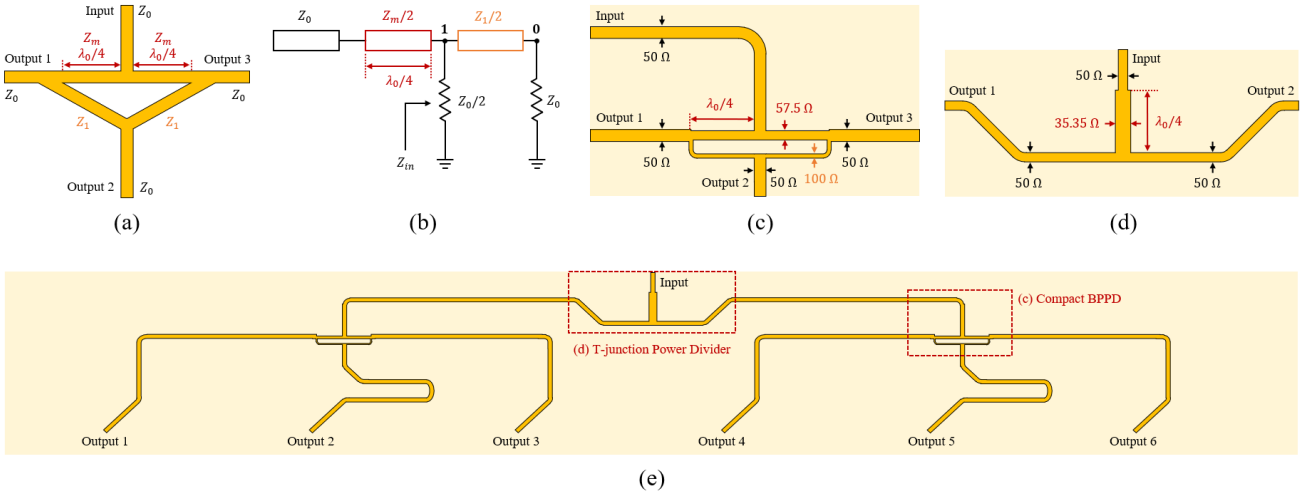

Figure 5. Geometry of the power dividers. (a) Schematic of the compact BPPD. (b) Equivalent circuit of the compact BPPD. (c) Compact 3-way BPPD. (d) 2-way T-junction power divider. (e) Proposed 6-way power divider.

As discussed in the introduction, the primary goal of the antenna design in this paper is to implement a high gain dual-polarized fan-beam antenna that focuses the signal within the Private 5G service area while minimizing the interference-sensitive zone in railway communications. In order to achieve a fan-beam pattern with a horizontal HPBW of 6° and a vertical HPBW of 40°, which provides balanced performance in practical railway communication environments, the proposed antenna elements are linearly arranged. The most important parameters in array antenna design are the number of antenna elements and the array spacing. Since the array beam pattern is given by the product of the antenna element beam pattern and the array factor, the desired array beam pattern can be achieved by arranging the number of elements and the array spacing[26,27]. However, as the array spacing increases, the grating lobes on the array factor appear in undesired directions, causing ambiguity issues in the array beam pattern[28]. Therefore, in most array antenna designs, the array spacing is strictly limited to $0.5\lambda_0$ or less, which is the condition where no grating lobes occur. On the other hand, since the proposed antenna element has a high gain and narrow beam pattern, even if grating lobes occur in undesired directions when arranged at a wide array spacing, they can be effectively suppressed by the antenna element pattern. Therefore, the proposed antenna is free from the constraints of array spacing to avoid grating lobe issues and offers the advantage of effectively achieving the desired array pattern simply by adjusting the array spacing. To achieve the design goal of a fan-beam pattern with horizontal HPBW of 6° and vertical HPBW of 40°, six proposed antenna elements with horizontal and vertical HPBW of 40° are arranged horizontally with an array spacing of $1.27\lambda_0$. In array antenna designs, doubling the number of antenna elements increases the gain by 3 dB and halves the HPBW. Therefore, implementing an array antenna with a HPBW of 6° requires a linear array of 16 conventional patch antenna elements with a HPBW of 100°. However, since the proposed antenna element has high gain and are free from the array spacing constraints, HPBW of 6° can be achieved with only six antenna elements.

To implement the proposed 6×1 array antenna, a non-binary power divider design is required, rather than a conventional 2-way power divider. Because the 2-way power divider has a simple structure and stable performance, the 2-way-based cascaded structure is commonly used for multi-way power dividing[29,30]. In contrast, non-binary power dividers have complex impedance design requirements, making their use limited to special purposes[31–33]. Since the proposed array antenna requires a 6-way power divider, a design approach is adopted to design a 3-way power divider and then integrate it into a 2-way T-junction power divider. In this paper, a compact Bagley Polygon power divider (BPPD) derived from an analytical model of the conventional BPPD is applied to the design of a 3-way power divider[34]. In conventional BPPD designs, the electrical line lengths between the three output ports of a 3-way power divider must be fixed to $0.5\lambda_0$ to ensure symmetry among the output ports. Due to this constraint, conventional BPPDs have the disadvantage of having output ports that spread radially and occupy a large area on the board. The compact BPPD design technique can maintain a constant input impedance regardless of the line length between output ports by setting the line impedance Z_1 between the output ports to $2Z_0$ based on the analytical model of the conventional BPPD. This setting allows arbitrary line length selection, which significantly reduces the board area compared to conventional BPPDs where the transmission line length is fixed to $0.5\lambda_0$. Fig. 5(a) and Fig. 5(b) illustrate the schematic of the compact BPPD and the equivalent circuit derived using symmetry, respectively. Referring to Fig. 5(b), when the characteristic impedance of the transmission line between nodes 0 and 1 satisfies the relationship $Z_1/2 = Z_0$, the input impedance Z_{in} becomes equal to Z_0

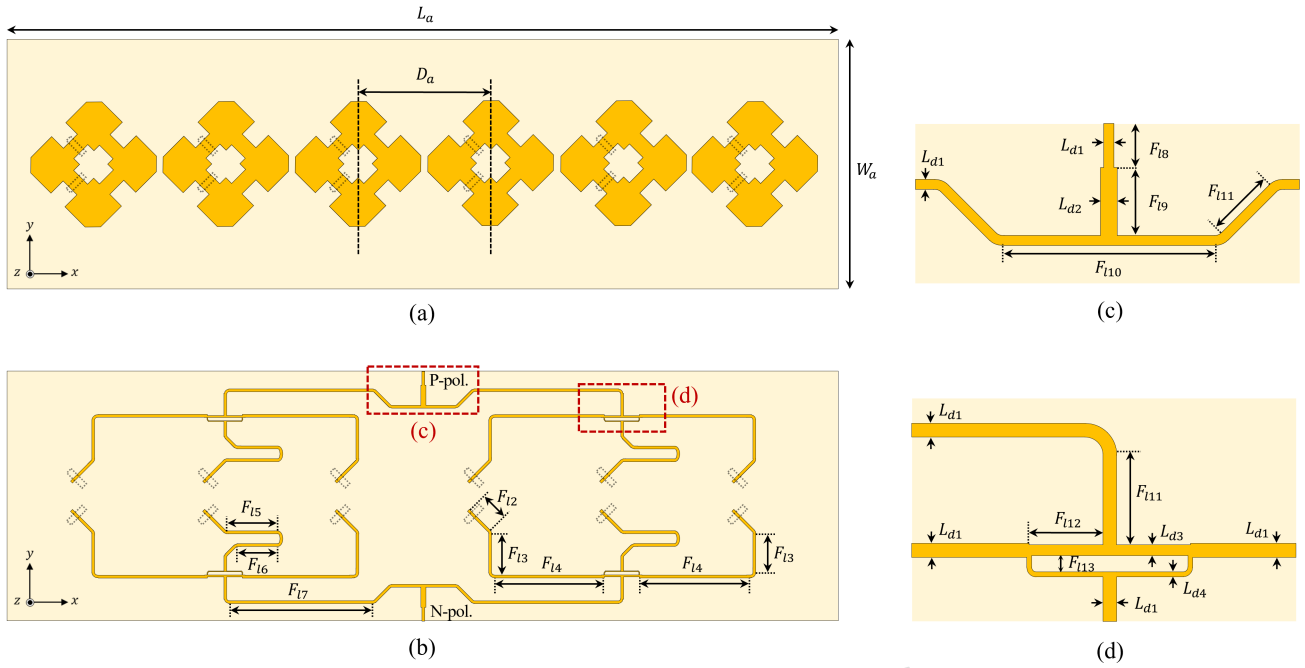

Figure 6. Geometry of the proposed array antenna. (a) Top view of the top layer. (b) Top view of the bottom layer. (c) 2-way T-junction power divider. (d) Compact 3-way BPPD. Parameters: $L_a = 500$, $W_a = 150$, $D_a = 80$, $F_{l1} = 17.6$, $F_{l2} = 22.48$, $F_{l3} = 66.54$, $F_{l4} = 29.4$, $F_{l5} = 23.45$, $F_{l6} = 85.76$, $F_{l7} = 8$, $F_{l8} = 12$, $F_{l9} = 35.51$, $F_{l10} = 11.66$, $F_{l11} = 9.63$, $F_{l12} = 2.11$, $F_{l13} = 11.97$, $L_{d1} = 1.84$, $L_{d2} = 3$, $L_{d3} = 1.46$, $L_{d4} = 0.58$ (unit: mm)

regardless of the line length. Therefore, the line length between output ports can be arbitrarily adjusted while the line width remains fixed. This structural flexibility allows the overall perimeter of the BPPD to be significantly reduced, allowing 3-way power dividing within a compact area. Fig. 5(c) and Fig. 5(d) illustrate the designs of the 3-way power divider and 2-way power divider, respectively. The 2-way power divider is designed simply using a quarter-wavelength transformer. The final 6-way power divider is designed by integrating two 3-way power dividers into a single 2-way power divider, as shown in Fig. 5(e). The proposed 6-way power divider does not require an additional impedance matching network, since the characteristic impedances of all input and output ports are designed to be 50Ω.

Fig. 6 illustrates the geometry of the proposed array antenna, which has the identical stacked structure as that shown in Fig. 1(a). In the top layer, in Fig. 6(a), six proposed antenna elements are arranged along the x-direction with an array spacing of 80 mm, corresponding to $1.27\lambda_0$. Although this wide array spacing causes grating lobes on the array factor at $\pm 52^\circ$, they are effectively suppressed because the antenna element has a HPBW of 40°. Therefore, there is no ambiguity issue due to the grating lobes. The inner layer contains ground slots arranged to excite dual-polarization (P-pol. and N-pol.) to each antenna element. The bottom layer in Fig. 6(b) has two 6-way power dividers to feed each polarization. The upper divider distributes power in six ways to excite the P-pol. ports of the six antenna elements, and the lower divider distributes power in six ways to excite the N-pol. ports. The 2-way T-junction power divider and the 3-way compact BPPD that comprise the 6-way power divider are illustrated in Fig. 6(c) and Fig. 6(d), respectively, and the design parameters are presented in the caption. All design parameters are optimized using a 3D EM simulator. The ground slots on the inner layer and the feed lines on the bottom layer feed the antenna elements through aperture coupling.

Experimental Results and Discussion

To verify the design feasibility of the proposed antenna element and array antenna, prototype antennas were fabricated and experimentally evaluated. The prototype antennas were constructed by vertically joining the upper substrate, supporting frame, and lower substrate using plastic bolts and nuts, ensuring a fully integrated multilayer PCB structure. This suspended structure, which maintains the air gap, plays an important role in achieving high gain performance by reducing the effective permittivity. An additional evaluation board was fabricated to verify the 6-way power divider for array antenna. This board was fabricated to verify the performance of the power divider in Fig. 6(b), and an experiment was conducted to determine whether the input

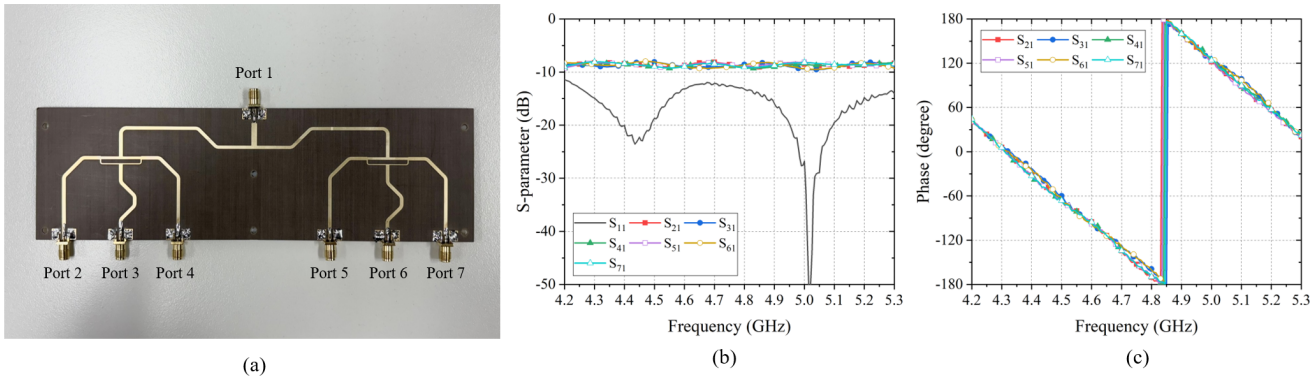

(a) (b) (c)

Figure 7. (a) Photograph of the fabricated 6-way power divider. (b) Measured reflection coefficient and insertion loss. (c) Measured insertion phase.

signal was evenly distributed with the same amplitude and phase to the six output ports. As shown in Fig. 7(a), the evaluation board for the 6-way power divider is implemented by integrating two 3-way compact BPPDs with a single 2-way T-junction power divider. The measured reflection coefficient, insertion loss, and insertion phase of the 6-way divider evaluation board are presented in Fig. 7(b) and Fig. 7(c), respectively. The measured results confirm that power is evenly distributed from the input port (Port 1) to the six output ports (Ports 2 to 7). The insertion loss deviation is within ±0.32 dB, and the insertion phase deviation is within ±2.8°, confirming that no pattern distortion occurs due to the amplitude and phase imbalance when feeding the array antenna. Fig. 8 presents the top and bottom views of the fabricated antenna element and array antenna. It can be seen that the physical implementation of the proposed antenna is identical to the simulation model.

The simulated and measured reflection coefficients and isolation between polarization ports of the prototype antenna element and array antenna are shown in Fig. 9. A vector network analyzer Anritsu MS46122B was used to measure the reflection coefficient. The simulated 10-dB impedance bandwidths of the proposed antenna element are 4.68-4.91 GHz for both N-pol. and P-pol., while the measured 10-dB impedance bandwidths are 4.43-4.92 GHz and 4.43-4.93 GHz for N-pol.

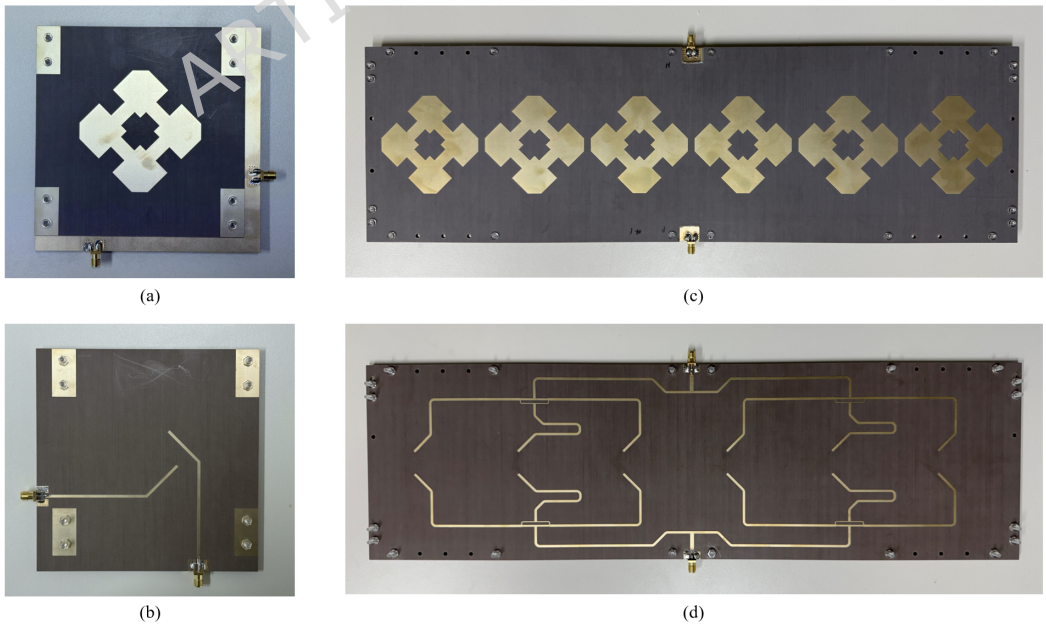

(a) (c)

(b) (d)

Figure 8. Photographs of the fabricated prototype antennas. (a) Top view and (b) bottom view of the prototype antenna element. (c) Top view and (d) bottom view of the prototype array antenna.

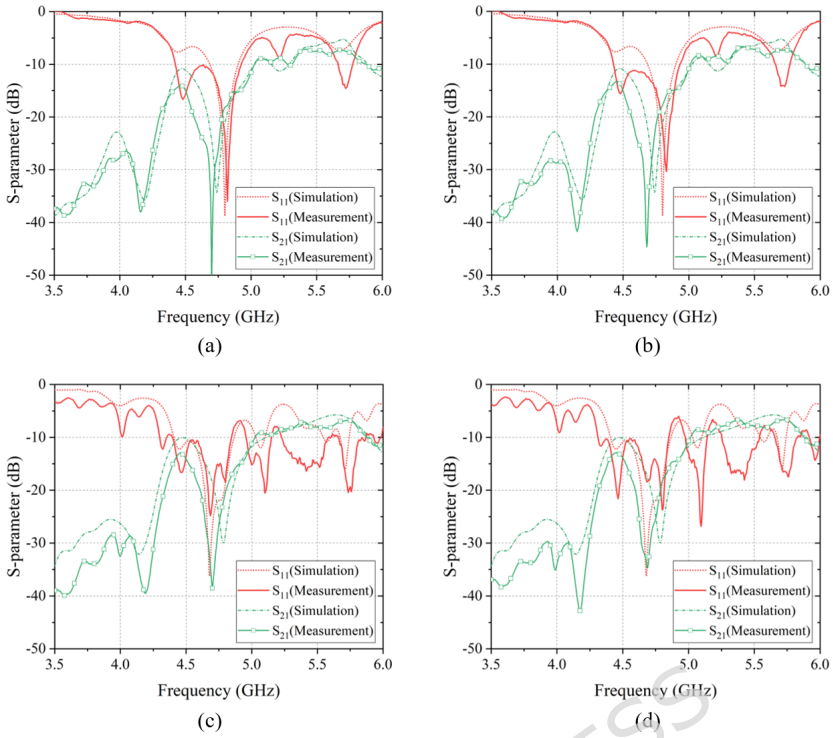

Figure 9. Simulated and measured reflection coefficient and isolation of the proposed antennas. (a) N-pol. and (b) P-pol. of the antenna element. (c) N-pol. and (d) P-pol. of the array antenna.

and P-pol. respectively. The simulated 10-dB impedance bandwidths of the proposed array antenna are 4.40-4.87 GHz for both N-pol. and P-pol., while the measured 10-dB impedance bandwidths are 4.30-4.85 GHz and 4.31-4.86 GHz for N-pol. and P-pol. respectively. The measured reflection coefficients of the prototype antennas show reasonable agreement with the simulated results. These results demonstrate that the operating characteristics of a single antenna element are well maintained in the array configuration without performance degradation caused by mutual coupling and resonant frequency shift. Furthermore, both the proposed antenna elements and array antenna have the bandwidth sufficient to cover the Private 5G band of 4.72-4.82 GHz, satisfying the specifications required for practical base station applications.

The radiation patterns of the prototype antennas were measured in the anechoic chamber at Soongsil University, and the

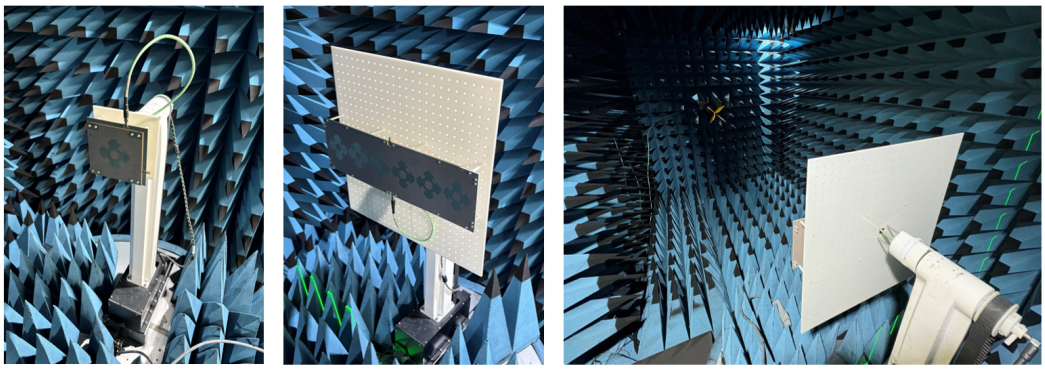

Figure 10. Radiation pattern measurement environment of the proposed antennas. (a) Antenna element. (b) Array antenna. (c) Aligned standard horn antenna and AUT.

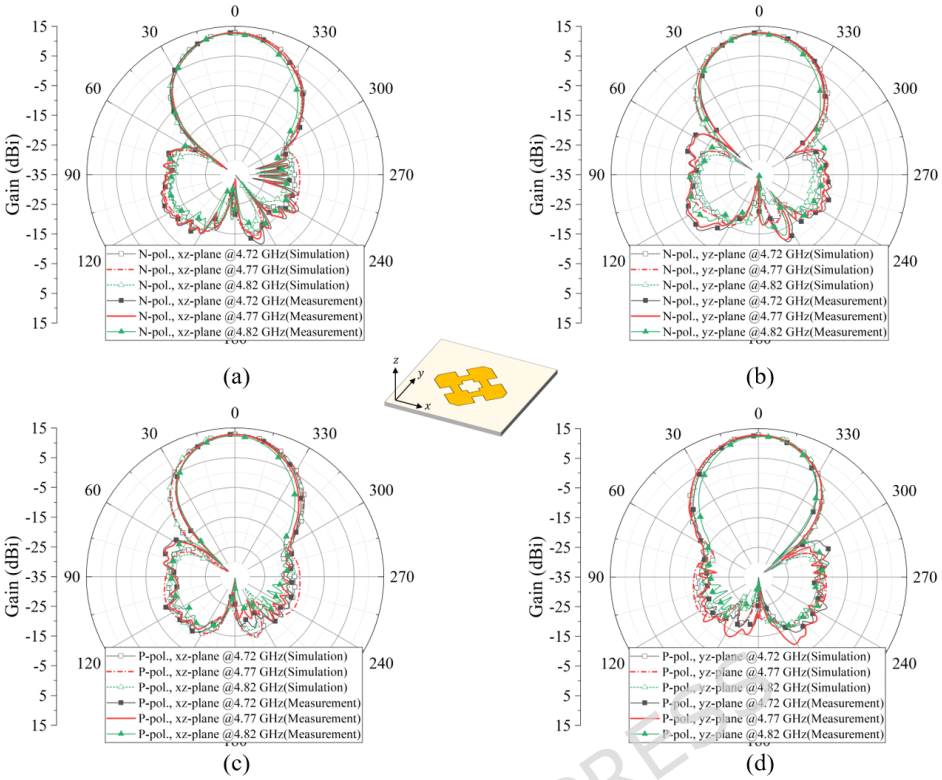

Figure 11. Simulated and measured radiation patterns of the proposed antenna element at 4.72, 4.77, and 4.82 GHz. (a) N-pol. in xz-plane. (b) N-pol. in yz-plane. (c) P-pol. in xz-plane. (d) P-pol. in yz-plane.

measurement environment is shown in Fig. 10. To accurately measure the slant dual-polarization characteristics, a reference horn antenna was installed at a 45° angle. A jig was designed and fabricated to align the central axes of the antenna under test (AUT) and the reference horn antenna. This precise alignment is essential for measuring dual-polarization characteristics and fan-beam patterns. The AUT was installed on a 360° rotating turntable to obtain radiation patterns over all elevation angles. The measurements were conducted at a sufficient distance to satisfy the far-field conditions, ensuring the reliability of the measurement data. Fig. 11 shows the simulated and measured xz-plane and yz-plane radiation patterns of the proposed antenna element for both polarizations at 4.72, 4.77, and 4.82 GHz. The patterns remain consistent over the three frequency points, confirming stable radiation characteristics across the entire Private 5G band. The simulation results of the proposed antenna element show a peak gain 12.9 dBi for both N-pol. and P-pol. with a balanced HPBW of 39.2°-39.8° in both xz-plane and yz-plane. The measured results show a peak gain of 12.8 dBi for both N-pol. and P-pol., and HPBW were similar to the simulation results in the 38.5°-39.2° range. This high level of agreement validates the antenna design process presented in the second section. It can be seen that the slots applied to higher-order mode patch antenna effectively suppress sidelobes and achieve high gain, and both polarizations show stable radiation performance with a peak gain of 12.8 dBi. The similar gain levels for both polarizations are crucial in Private 5G base stations, as they provide a foundation for maintaining stable link quality even in NLoS scenarios, where the polarization state frequently varies.

The simulated and measured radiation patterns of the 6×1 array antenna are presented in Fig. 12 at 4.72, 4.77, and 4.82 GHz. The results show that the fan-beam radiation characteristics are maintained with good agreement between simulation and measurement across the entire band. The simulated results of the proposed array antenna show a peak gain of 18.8 dBi for both N-pol. and P-pol., a narrow HPBW of 5.9° in the xz-plane and a HPBW of 39° in the yz-plane. The measured results were consistent with the simulated results, demonstrating a peak gain of 18.6 dBi for both polarizations, and HPBWs of 6° in the xz-plane and 38° in the yz-plane. The measured radiation patterns of the proposed array antenna validate the array design presented in the second section. It can be seen that the fan-beam patterns are achieved without grating lobe issues even though the array spacing is set to $1.27\lambda_0$ because the antenna elements have high gain. Furthermore, the proposed array antenna has high gain, dual-polarization, and a fan-beam pattern despite its overall size of 500×150 mm^2, with a diagonal length of $1.21\lambda_0$, significantly improving its practicality for Private 5G base stations. This is because the antenna elements used in the array have

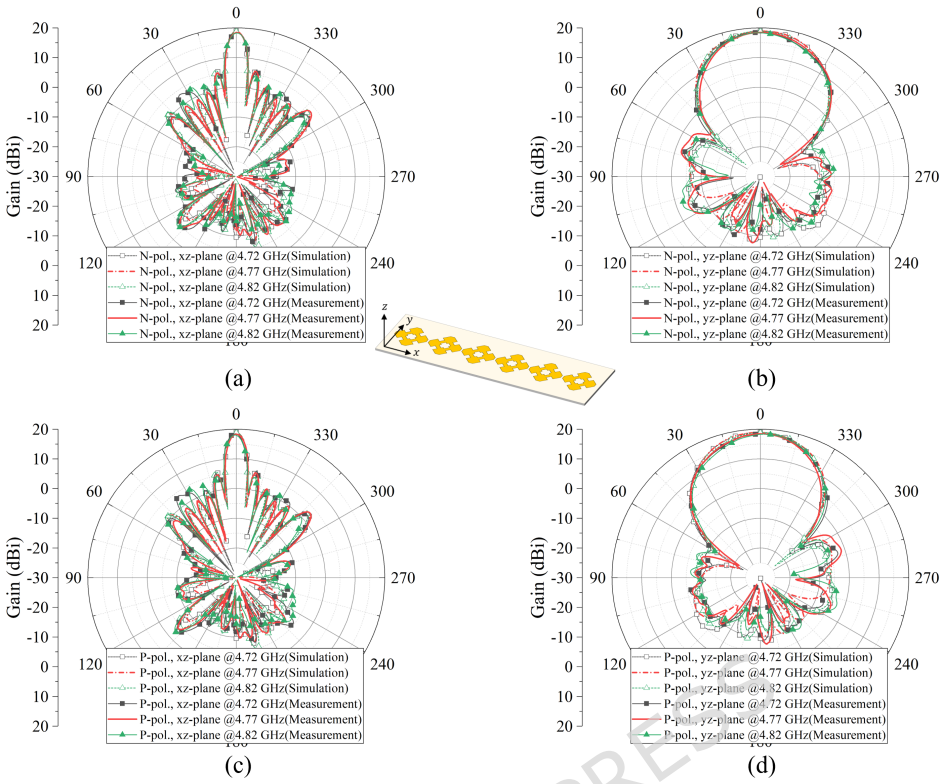

Figure 12. Simulated and measured radiation patterns of the proposed array antenna at 4.72, 4.77, and 4.82 GHz. (a) N-pol. in xz-plane. (b) N-pol. in yz-plane. (c) P-pol. in xz-plane. (d) P-pol. in yz-plane.

relatively high gain and wide bandwidth compared to the physical size. While many high gain antennas suffer from trade-offs such as increased size or reduced bandwidth to achieve high gain, the proposed antenna achieves balanced performance by maintaining both sufficient bandwidth and high gain within a relatively small size. To quantitatively compare the performance balance of the proposed antenna with previous works, the following figure of merit (FoM) is introduced in this study.

$$FoM = \frac{G \times BW}{L_d} \tag{2}$$

The FoM consists of the peak gain (G), fractional bandwidth (BW), and the diagonal length (L_d), which is the maximum length of the radiating element. Defining bandwidth as a fractional bandwidth rather than an absolute bandwidth allows for consistent performance comparisons across different frequency bands. This metric is designed to have higher values for smaller antennas, wider bandwidths, and higher gains, providing an objective measure for fairly comparing the balanced performance

Ref.	Center Frequency	Polarization	Fractional Bandwidth	Diagonal Length	Peak Gain	FoM
18	3.7 GHz	Dual pol.	4.32%	$1.07\lambda_0$	10.5 dBi	42.39
19	5.96 GHz	Dual pol.	3.02%	$1.28\lambda_0$	10.9 dBi	25.80
20	12.52 GHz	Dual pol.	2.32%	$2.63\lambda_0$	15.5 dBi	13.67
21	4.77 GHz	Dual pol.	1.88%	$1.16\lambda_0$	12.5 dBi	20.28
This Work	**4.77 GHz**	**Slant Dual pol.**	**4.50%**	$\mathbf{1.21\lambda_0}$	**12.8 dBi**	**47.52**

Table 1. Performance comparison between the proposed antenna element and the previous works.

of antennas. Table 1 presents the performance comparison between the proposed antenna element and previous works. The antennas reported in reference[18] and[19] exhibit balanced performance in terms of size, gain, and bandwidth, but their gain levels remain relatively low. The antenna reported in reference[20] exhibits high gain, but its large size and narrow bandwidth significantly limit its practical applicability. The antenna reported in reference[21] exhibits high gain relative to its size, but its narrow bandwidth makes it less suitable for practical applications. The antenna proposed in this study achieves the highest FoM by simultaneously achieving a diagonal length of $1.21\lambda_0$, a fractional bandwidth of 4.50%, and a peak gain of 12.8 dBi at a center frequency of 4.77 GHz. The proposed antenna achieves an FoM value of 47.52, overcoming the limitations of previous works in which practical applicability was constrained by the large size or narrow bandwidth. This is interpreted as the result of an optimized design that effectively utilizes the structural improvements presented during the design process. Furthermore, this balanced performance will serve as the foundation for high reliability in both LoS and NLoS environments when applied to Private 5G base stations. It is expected to provide excellent performance in terms of coverage, interference control, and link stability required in practical railway communications.

Conclusion

In this paper, a novel antenna structure that simultaneously satisfies high gain, dual-polarization, and fan-beam characteristics is proposed for next-generation Private 5G base stations for railway communications. The proposed antenna element effectively overcomes the gain limitations of conventional rectangular patch-based dual-polarization antennas by utilizing a radiation mechanism derived from a higher-order mode patch antenna and a sidelobe suppression technique using center and side slots. It achieves a high gain of 12.8 dBi and stable radiation performance despite its relatively small size. The proposed antenna element achieves slant dual-polarization characteristics by rotating the antenna element by 45°, providing robustness against polarization variations frequently encountered in practical railway communication environments and ensuring the reliability required for Private 5G base stations. In addition, an array antenna was constructed by linearly arranging six proposed antenna elements to implement a fan-beam radiation pattern that can provide balanced performance in both LoS and NLoS environments. The grating lobe issue, which occurs in conventional patch-based array antennas, was effectively suppressed by the high gain characteristic of the proposed antenna element, and stable beam patterns are maintained even when the array spacing is extended to $1.27\lambda_0$. To feed the proposed array antenna, a 6-way power divider was designed by combining a compact 3-way BPPD with a 2-way T-junction power divider. The uniform power dividing performance was experimentally verified. Measurement results of the fabricated prototype array antenna demonstrated a high gain of 18.6 dBi and fan-beam pattern, satisfying the design objectives. Both the proposed antenna element and array antenna achieved bandwidths sufficient to cover the Private 5G band, ensuring performance suitable for practical base stations. Finally, through a FoM comparison introduced to quantitatively evaluate the antenna's balanced performance, the proposed antenna exhibits improved balance among size, gain, and bandwidth compared to previously reported antennas. These performance advantages and structural efficiency suggest that the proposed antenna structure not only meets the practical requirements of a Private 5G-R base station antenna, but also offers high scalability for application in various high frequency wireless communication systems. Future research is expected to further the proposed design through expansion of the array structure, integration of beamforming functions, and field test in actual railway communication systems.

References

1. He, R. *et al.* 5g for railways: Next generation railway dedicated communications. *IEEE Commun. Mag.* **60**, 130–136, DOI: 10.1109/MCOM.005.2200328 (2022).

2. Lee, S.-Y. Private 5g (e-um 5g) trend and promotion policy. *The J. Korean Inst. Electromagn. Eng. Sci.* **33**, 531–540, DOI: 10.5515/KJKIEES.2022.33.7.531 (2022).

3. Ai, B., Molisch, A. F., Rupp, M. & Zhong, Z.-D. 5g key technologies for smart railways. *Proc. IEEE* **108**, 856–893, DOI: 10.1109/JPROC.2020.2988595 (2020).

4. He, R. *et al.* Radio communication scenarios in 5g-railways. *China Commun.* **20**, 235–246, DOI: 10.23919/JCC.ea.2021-0296.202302 (2023).

5. Sharma, S., Ganguly, C. & De, S. Effect of polarization on rf signal transmission over two-ray channel. In *2023 National Conference on Communications (NCC)*, 1–6, DOI: 10.1109/NCC56989.2023.10068000 (2023).

6. Lempianen, J., Laiho-Steffens, J. & Wacker, A. Experimental results of cross polarization discrimination and signal correlation values for a polarization diversity scheme. In *1997 IEEE 47th Vehicular Technology Conference. Technology in Motion*, vol. 3, 1498–1502 vol.3, DOI: 10.1109/VETEC.1997.605617 (1997).

7. Gao, M. *et al.* Dynamic mmwave beam tracking for high speed railway communications. In *2018 IEEE Wireless Communications and Networking Conference Workshops (WCNCW)*, 278–283, DOI: 10.1109/WCNCW.2018.8368998 (2018).

8. Farasat, M., Thalakotuna, D. N., Hu, Z. & Yang, Y. A review on 5g sub-6 ghz base station antenna design challenges. *Electronics* **10**, DOI: 10.3390/electronics10162000 (2021).

9. Muhammad Hussain, K. L. & Kim, D. Tapered high-gain fabry-perot cavity antenna with high sidelobe suppression for 5g industry. *Sci. Reports* **13**, 15744, DOI: 10.1038/s41598-023-42716-8 (2023).

10. Ahamed, M. M. & Faruque, S. 5g network coverage planning and analysis of the deployment challenges. *Sensors* **21**, DOI: 10.3390/s21196608 (2021).

11. Debaprasad Barad, D. S., Jogesh Chandra Dash & Srinivasulu, P. Dual-band dual-polarized sub-6 ghz phased array antenna with suppressed higher order modes. *Sci. Reports* **14**, 6139, DOI: 10.1038/s41598-024-56218-8 (2024).

12. Chiaraviglio, L., Rossetti, S., Saida, S., Bartoletti, S. & Blefari-Melazzi, N. "pencil beamforming increases human exposure to electromagnetic fields": True or false? *IEEE Access* **9**, 25158–25171, DOI: 10.1109/ACCESS.2021.3057237 (2021).

13. Gajšek, P., Apostolidis, C., Plets, D., Samaras, T. & Valič, B. Emf exposure of workers due to 5g private networks in smart industries. *Electronics* **14**, DOI: 10.3390/electronics14132662 (2025).

14. Wu, S. & Shang, F. Broadband dual-polarized magnetoelectric dipole antenna with compact structure for 5g base station. *IEEE Access* **11**, 20806–20813, DOI: 10.1109/ACCESS.2023.3247821 (2023).

15. Feng, L. Y. & Zhang, C. Q. Compact magneto-electric dipole director loaded high-gain dual-polarized magneto-electric dipole antenna. *IEEE Antennas Wirel. Propag. Lett.* **23**, 2130–2134, DOI: 10.1109/LAWP.2024.3382879 (2024).

16. Zhu, Y.-Y., Wang, J., Chen, J.-X. & Wu, W. A compact wideband dual-polarized antenna using monolithic dielectric for 5g base station application. *IEEE Antennas Wirel. Propag. Lett.* **21**, 1717–1721, DOI: 10.1109/LAWP.2022.3173085 (2022).

17. Tang, H., Deng, X. & Shi, J. Wideband substrate integrated differential dual-polarized dielectric resonator antenna. *IEEE Antennas Wirel. Propag. Lett.* **21**, 203–207, DOI: 10.1109/LAWP.2021.3125100 (2022).

18. Gao, Y., Ma, R., Wang, Y., Zhang, Q. & Parini, C. Stacked patch antenna with dual-polarization and low mutual coupling for massive mimo. *IEEE Transactions on Antennas Propag.* **64**, 4544–4549, DOI: 10.1109/TAP.2016.2593869 (2016).

19. He, Y., Li, Y., Sun, W., Zhang, Z. & Chen, P.-Y. Dual linearly polarized microstrip antenna using a slot-loaded tm50 mode. *IEEE Antennas Wirel. Propag. Lett.* **17**, 2344–2348, DOI: 10.1109/LAWP.2018.2874472 (2018).

20. He, Y., Li, Y., Sun, W. & Zhang, Z. Dual-polarized, high-gain, and low-profile magnetic current array antenna. *IEEE Transactions on Antennas Propag.* **67**, 1312–1317, DOI: 10.1109/TAP.2018.2883609 (2019).

21. Chen, C. A single-layer single-patch dual-polarized high-gain cross-shaped microstrip patch antenna. *IEEE Antennas Wirel. Propag. Lett.* **22**, 2417–2421, DOI: 10.1109/LAWP.2023.3289861 (2023).

22. Luo, Y., Chu, Q.-X. & Wen, D.-L. A plus/minus 45 degree dual-polarized base-station antenna with enhanced cross-polarization discrimination via addition of four parasitic elements placed in a square contour. *IEEE Transactions on Antennas Propag.* **64**, 1514–1519, DOI: 10.1109/TAP.2016.2522463 (2016).

23. Quan, X., Li, R., Fan, Y. & Anagnostou, D. E. Analysis and design of a 45 ° slant-polarized omnidirectional antenna. *IEEE Transactions on Antennas Propag.* **62**, 86–93, DOI: 10.1109/TAP.2013.2288367 (2014).

24. Zakerifar, H., Nourinia, J. & Ghobadi, C. Broadband dual-polarized antenna with parasitic elements for base-station applications. *Int. J. Microw. Wirel. Technol.* **16**, 1272–1282, DOI: 10.1017/S175907872400103X (2024).

25. Balanis, C. A. *Antenna Theory: Analysis and Design* (John Wiley & Sons, Hoboken, NJ, 2016), 4th edn.

26. Mailloux, R. J. *Phased Array Antenna Handbook* (Artech House, Norwood, MA, 2017), 3rd edn.

27. Stutzman, W. L. & Thiele, G. A. *Antenna Theory and Design* (John Wiley & Sons, Hoboken, NJ, 2012), 3rd edn.

28. Ahn, B. *et al.* Wide-angle scanning phased array antenna using high gain pattern reconfigurable antenna elements. *Sci. Reports* **9**, 18391, DOI: 10.1038/s41598-019-54120-2 (2019).

29. Wilkinson, E. An n-way hybrid power divider. *IRE Transactions on Microw. Theory Tech.* **8**, 116–118, DOI: 10.1109/TMTT.1960.1124668 (1960).

30. Pozar, D. M. *Microwave Engineering* (John Wiley & Sons, Hoboken, NJ, 2011), 4th edn.

31. Choe, W. & Jeong, J. *n*-way unequal wilkinson power divider with physical output port separation. *IEEE Microw. Wirel. Components Lett.* **26**, 243–245, DOI: 10.1109/LMWC.2016.2537043 (2016).

32. Ahn, S.-h., Lee, J. W., Cho, C. S. & Lee, T. K. A dual-band unequal wilkinson power divider with arbitrary frequency ratios. *IEEE Microw. Wirel. Components Lett.* **19**, 783–785, DOI: 10.1109/LMWC.2009.2033503 (2009).

33. Chen, H., Zhang, T., Che, W., Feng, W. & Xue, Q. Unequal wilkinson power divider with wide range of arbitrary power division based on recombinant technology. *IET Microwaves, Antennas & Propag.* **9**, 166–175, DOI: 10.1049/iet-map.2014.0304 (2015).

34. Sakagami, I., Wuren, T., Fujii, M. & Tahara, M. Compact multi-way power dividers similar to the bagley polygon. In *2007 IEEE/MTT-S International Microwave Symposium*, 419–422, DOI: 10.1109/MWSYM.2007.380477 (2007).

Author contributions statement

J.-G. L. conducted design and simulations, J.-G. L. and Y. H. conducted experiments, J.-G. L. and B. K. A. analyzed the data and wrote the manuscript. All authors reviewed the manuscript.

Competing interests

The authors declare no competing interests.

Funding

The authors received no funding for this work.

Data availability

The datasets used and analyzed during the current study are available from the corresponding author on reasonable request.

Additional information

Correspondence and requests for materials should be addressed to B. K. A.